Experimental Thermal and Fluid Science 63 (2015) 133–143

Contents lists available at ScienceDirect

Experimental Thermal and Fluid Science

journal homepage: www.elsevier.com/locate/etfs

Negative surges and unsteady turbulent mixing induced by rapid gate opening in a channel

Xinqian Leng, Hubert Chanson *

The University of Queensland, School Civil Engineering, Brisbane, QLD 4072, Australia

ARTICLE INFO

Article history:
Received 27 March 2014
Received in revised form 14 June 2014
Accepted 14 June 2014
Available online 23 June 2014

Keywords:
Negative surges
Physical modelling
Bed roughness
Free-surface measurements
Unsteady turbulent mixing
Velocity measurements
Reynolds stresses
Ensemble-average

ABSTRACT

A negative surge is an unsteady open channel flow characterised by a drop in water surface elevation. In this study, a negative surge generated by the rapid gate opening was investigated experimentally with three types of bed roughness. Both instantaneous free-surface and velocity measurements were performed and the results were ensemble-averaged. The experimental data showed a rapid flow acceleration beneath the negative surge, and large and rapid fluctuations in all instantaneous velocity components were observed during the passage of the negative surge leading edge. The Reynolds stress data showed large ensemble-average and fluctuation levels, significantly larger than in the initially steady flow, occurring slightly after the passage of the surge leading edge. The time difference between the maximum Reynolds stress and surge leading edge was observed to increase with increasing distance from the gate, and it was comparable to the time delay for the occurrence of maximum free-surface fluctuations. The findings suggested that the unsteady flow properties were little affected by the bed roughness, despite the broad range of equivalent sand roughness heights tested herein.

© 2014 Elsevier Inc. All rights reserved.

1. Introduction

In an open channel, the operation of a regulation structure (e.g. gate) is typically associated with a lowering of the water level on one side and the rise in water elevation on the other side. These unsteady processes are called respectively negative surge and positive surge. They are commonly observed in water supply channels during the operation of regulations gates (Fig. 1). Although there is an extensive literature dealing with their steady flow operation [19,11,22], limited information is available on the transient operation of gates. Fig. 2 illustrates the generation of negative surges caused by gate operation.

Negative surges may be analysed using the Saint-Venant equations and the method of characteristics in channels of relatively simple geometry. The Saint-Venant equations are one-dimensional unsteady open channel flow equations characterising the variations in space and time of the water depth d and flow velocity V:

$$B \times \frac{\partial d}{\partial t} + A \times \frac{\partial V}{\partial x} + B \times V \times \frac{\partial d}{\partial x} + V \times \left(\frac{\partial A}{\partial x}\right)_{d=\text{constant}} = 0 \qquad (1)$$

$$\frac{\partial V}{\partial t} + V \times \frac{\partial V}{\partial x} = -g \times \frac{\partial d}{\partial x} + g \times (S_o - S_f) \qquad (2)$$

where x is the longitudinal co-ordinate positive downstream, A is the flow cross-section area, B is the free-surface width, g is the gravity acceleration, S_o is the bed slope and S_f is the friction slope [20,3]. Several textbooks presented the complete solutions of negative surges propagating in prismatic rectangular channels [11,23,29]. Experimental studies included the free-surface measurements of [7], and the unsteady velocity data of [26]. Numerical studies of negative surges are more numerous [27,30], albeit restricted by the limited amount of detailed validation data sets.

In this contribution, a physical study is presented with a focus on the unsteady turbulent mixing during a negative surge propagating upstream following a rapid gate opening. Detailed measurements were performed in a relatively large facility with three types of bottom roughness. Both instantaneous free-surface and velocity measurements were conducted and the results were ensemble-averaged. It is the purpose of this contribution to study thoroughly the upstream surge propagation and associated turbulent mixing, including the impact of bed roughness.

2. Physical modelling of negative surges and instrumentation

2.1. Presentation

Physical models are commonly used in hydraulic engineering to optimise a structure. In a laboratory model, the flow conditions

* Corresponding author. Tel.: +61 7 33653516; fax: +61 7 33 65 45 99.
E-mail address: h.chanson@uq.edu.au (H. Chanson).
URL: http://www.uq.edu.au/~e2hchans/ (H. Chanson).

http://dx.doi.org/10.1016/j.expthermflusci.2014.06.015
0894-1777/© 2014 Elsevier Inc. All rights reserved.

Fig. 1. Fully-opened radial gates along the Toyohashi-Tahara aqueduct, Toyohashi City (Japan) on 26 November 1998.

must be similar to those in the prototype: that is, geometric, kinematic and dynamic similarities must be fulfilled. In a dimensional analysis, the relevant parameters include the fluid properties and physical constants, the channel geometry and initial flow conditions, and the unsteady flow properties. Considering the simple case of a negative surge propagating in a rectangular, horizontal channel after a sudden and complete gate opening, a dimensional analysis yields:

$$\frac{d}{d_o},\frac{P}{\rho\times g\times d_o},\frac{V_x}{V_o},\frac{V_y}{V_o},\frac{V_z}{V_o} = F\left(\frac{x}{d_o},\frac{y}{d_o},\frac{z}{d_o},t\times\sqrt{\frac{g}{d_o}},\frac{V_o}{\sqrt{g\times d_o}},\rho\times\frac{V_o\times d_o}{\mu},\frac{g\times\mu^4}{\rho\times\sigma^3},\frac{B}{d_o},\frac{k_s}{d_o},\ldots\right) \quad (3)$$

where d is the flow depth, P is the instantaneous pressure at a location (x, y, z) and time t, V_x, V_y, V_z are respectively the instantaneous longitudinal, transverse and vertical velocity components, x is the streamwise coordinate in the flow direction, y is the horizontal transverse coordinate measured from the channel centreline, z is the vertical coordinate measured from channel bed, t is the time, d_o and V_o are the initial flow depth and velocity respectively, B is the channel width, k_s is the equivalent sand roughness height of the bed, g is the gravity acceleration, ρ and μ are the water density and dynamic viscosity respectively, and σ is the surface tension between air and water. Eq. (3) describes the dimensionless unsteady turbulent flow properties at a position and time as functions of a number of dimensionless parameters, including the Froude number (5th term), the Reynolds number (6th term) and the Morton number (7th term). Note that the effects of surfactants and biochemicals were neglected in the above development.

Herein a Froude similitude was applied and the experiments were conducted in a large size facility operating at large Reynolds numbers. These conditions may correspond to a 1:10 scale study of the channel shown in Fig. 1, thus ensuring that the extrapolation of the laboratory data to prototype conditions is unlikely to be adversely affected by scale effects.

2.2. Experimental facility and instrumentation

The experiments were conducted in a horizontal rectangular flume. The channel test section was 12 m long 0.5 m wide, made of smooth PVC bed and glass walls. The water was supplied by a constant head tank feeding a 2.1 m long 1.1 m wide 1.1 m deep intake basin, leading to the test section through a bed and sidewall convergent. A tainter gate was located next to the downstream end $x = x_{Gate} = 11.12$ m where x is the distance from the channel test section upstream end. This channel was previously used to study positive surges [5,13].

The water discharge was measured with an orifice meter designed based upon the British Standards [2] and calibrated on site with a V-notch weir. The percentage of error was expected to be less than 2%. In steady flows, the water depths were measured using rail mounted pointer gauges. The unsteady flow depths were recorded with a series of acoustic displacement meters Microsonic™ Mic+25/IU/TC located along and above the channel. The acoustic displacement meters were calibrated against the pointer gauges in steady flows and their accuracy was 0.2 mm. Note herein that the water depths were measured above the top of the rubber mats ($z = 0$) as shown in Fig. 3, in line with studies of d-type roughness [6]. The assumption was supported by visual observations suggesting zero to negligible flow motion through the mats.

The velocity measurements were conducted with an acoustic Doppler velocimeter Nortek™ Vectrino+(Serial No. VNO 0436) equipped with a three-dimensional side-looking head. The velocity range was ±1.0 m/s, the sampling rate was 200 Hz, and the data accuracy was 1% of the velocity range. Both the acoustic displacement meters and acoustic Doppler velocimeter were synchronised within ±1 ms and were sampled simultaneously at 200 Hz. The translation of the ADV probe in the vertical direction was controlled by a fine adjustment travelling mechanism connected to a MitutoyoTM digimatic scale unit. The error on the vertical position of the probe was $\Delta z < 0.025$ mm. The accuracy on the longitudinal position was estimated as $\Delta x < \pm 2$ mm. Herein all the measurements were taken on the channel centreline. Additional information was obtained with some digital still cameras Panasonic™ DMC-FX36 and Pentax™ K-7, and video camera

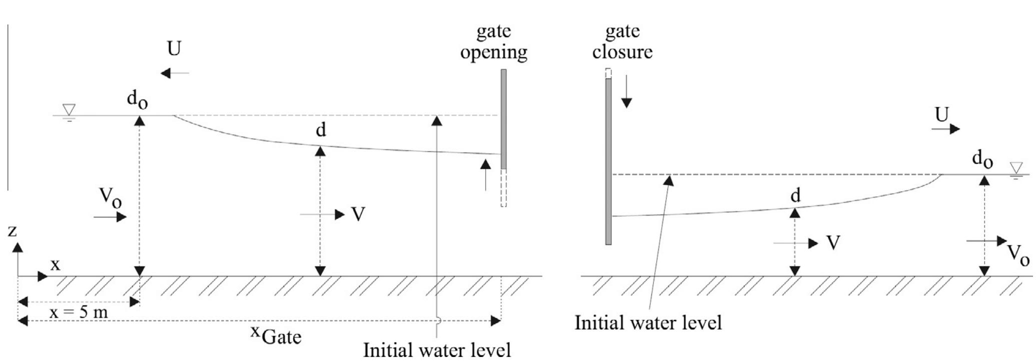

Fig. 2. Definition sketch of negative surges induced by gate operation: upstream surge propagation (left) and downstream surge propagation (right).

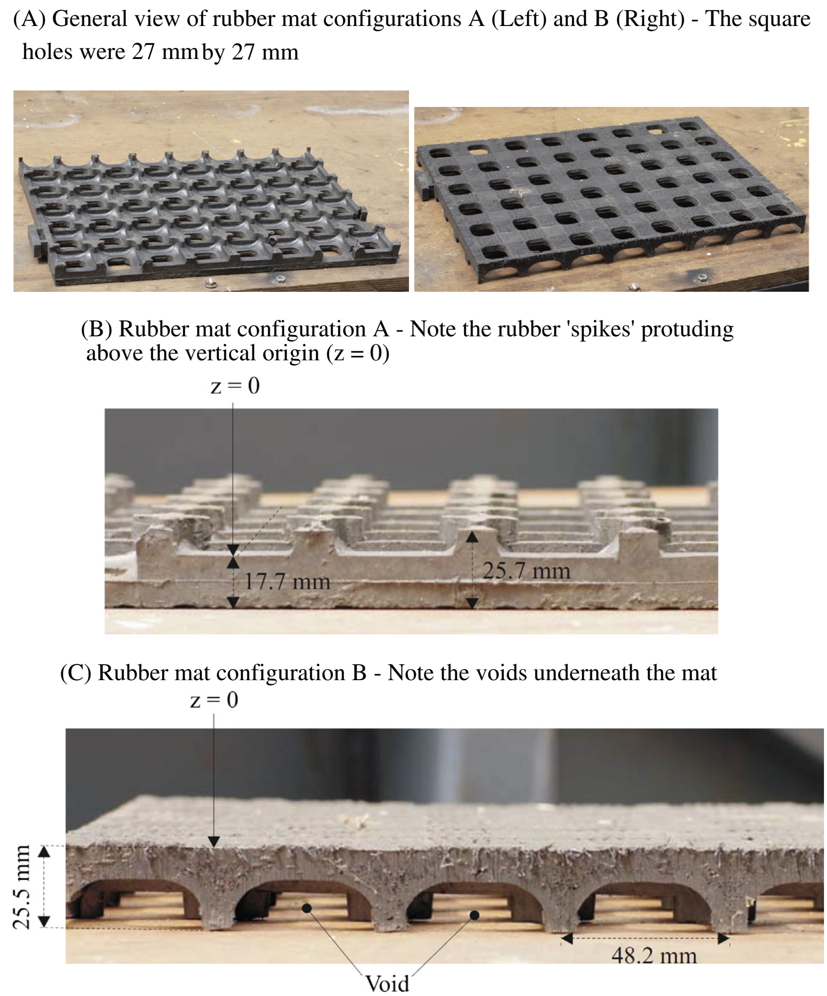

Fig. 3. Rubber mat configurations.

Sony™ HDR-XR160E (50fps, resolution: 1920p × 1080p). Further details were reported in [18].

2.3. ADV signal processing

For all experiments, the present experience highlighted some problems with the ADV velocity data, including low correlations and low signal to noise ratios. Initially this was primarily caused by some inadequate seeding of the channel water. The channel was seeded thereafter with a dilution of spherical glass powder, of approximately 100 g of glass powder diluted in 5 l of water for every hour of channel operation. The glass bead solution was introduced in the intake structure and dispersed progressively with time.

The post processing of the ADV data was conducted with the software WinADV™ version 2.028 using a similar method to Koch and Chanson [15]. In steady flows, the ADV post processing included the removal of communication errors, the removal of average signal to noise ratio data less than 5 dB and the removal of average correlation values less than 60%. In addition, the phase-space thresholding technique developed by Goring and Nikora [8] and implemented by Wahl [31] was used to remove spurious points in the data set. In unsteady flow conditions, the above post-processing technique was not applicable, because it cannot differentiate between unsteady fluctuations and spurious spikes (NIKORA 2004, *Person. Comm.*; [15]). The unsteady flow post-processing was limited to a removal of RS-232 communication errors, and it is acknowledged that the vertical velocity component V_z data might be affected adversely by the bed proximity for $z < 0.030$ m.

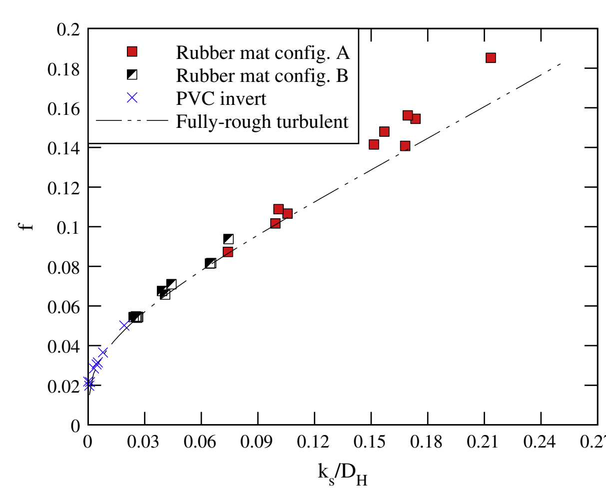

Fig. 4. Darcy-Weisbach friction factor data of the PVC bed and rubber mat configurations – comparison with Karman-Prandtl resistance equation for turbulent flow in rough pipes (Eq. (4)).

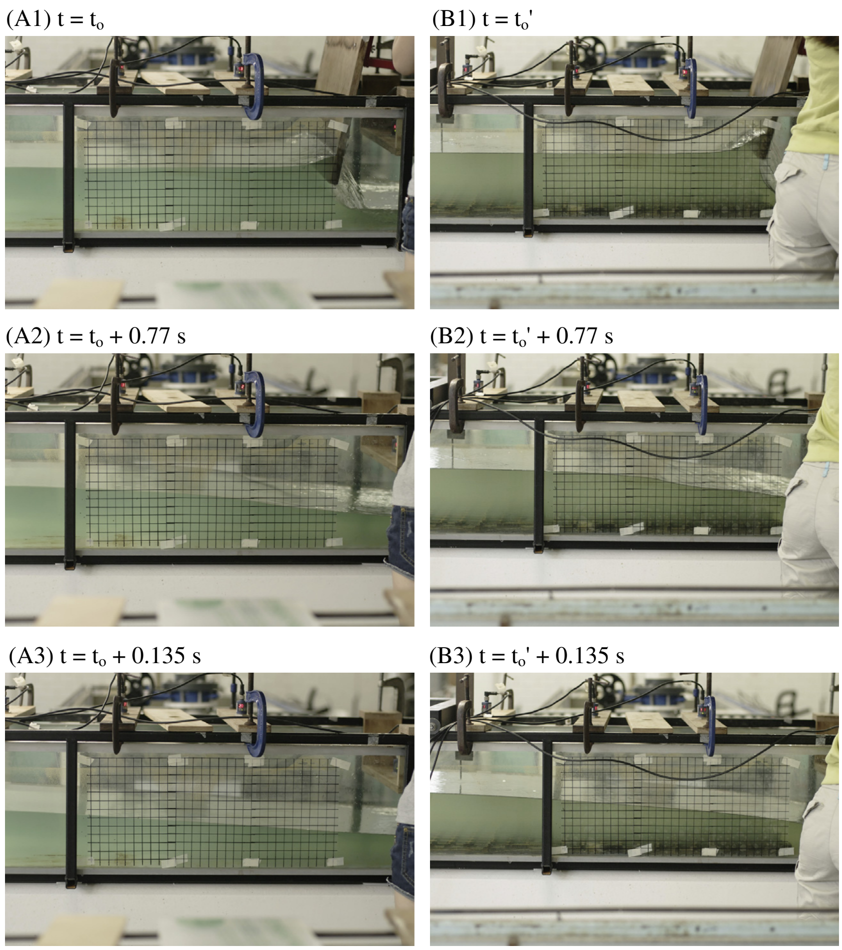

Fig. 5. Negative surge generation immediately upstream of the gate – initial flow direction from left to right, surge propagation from right to left – flow conditions: Q = 0.0254 m^3/s, d_o = 0.155 m – (A, left): smooth bed configuration; (B, right): rough bed (rubber mat configuration A).

2.4. Bed configurations and characteristics

Three types of bed roughness were tested systematically. Some experiments were performed with the smooth PVC invert. For others, the smooth PVC channel bed was covered with a series of industrial rubber floor mats for $0.075 < x < 11.10$ m. The rubber mats consisted of square patterns (Fig. 3), cut to the channel width and laid on the PVC. Each side was tested: configurations A and B. The configuration B corresponded to the conventional floor mat setting, allowing some continuous gaps between the PVC and rubber floor. With that configuration B, some seepage flow was observed through the rubber mat floor and the hydraulic conductivity of the material was tested. The results yielded a hydraulic conductivity $K \approx 0.14$ m/s and permeability $k \approx 1.4 \times 10^{-8}$ m^2, comparable to the properties of crushed rockfill [25,4].

The hydraulic roughness of the PVC invert and rubber mat configurations was tested for a range of steady flow conditions with discharges ranging from 0.006 to 0.030 m^3/s. The Darcy–Weisbach friction factor of PVC bed ranged from 0.020 to 0.050 corresponding to mean equivalent sand roughness height $k_s \approx 1$ mm. The

Table 1
Unsteady free-surface and velocity measurements in negative surges.

Reference	Q (m^3/s)	Bed roughness	h (m)	d_o (m)	U (m/s)	$\rho \times \frac{V_o \times d_o}{\mu}$	Instrumentation
Reichstetter and Chanson [26]	0.020 & 0.030	PVC	0.030–0.050	0.10–0.26	0.25–0.91 (^{1})	4.0×10^4 & 6.0×10^4	Video imagery
	0.020	PVC	0.030	0.24	0.91 (^{1})	4.0×10^4	Acoustic displacement meters & ADV Vectrino+
Present study	0.025	PVC	0.045–0.070	0.107–0.23	0.5–1.25 (^{2})	5.0×10^4	Acoustic displacement meters & ADV Vectrino+
	0.035		0.075–0.090	0.128–0.181	0.53–0.94	6.8×10^4	(x = 5 & 10.9 m)
	0.025	Rubber mat config. A	0.060–0.073	0.156–0.222	1.01 to 1.41	5.0×10^4	Acoustic displacement meters & ADV Vectrino+
	0.035		0.085–0.092	0.180–0.210	0.83–1.11	6.8×10^4	(x = 5 & 10.9 m)
	0.025	Rubber mat config. B	0.060 to 0.070	0.15–0.23	0.81–1.09	5.0×10^4	Acoustic displacement meters & ADV Vectrino+
	0.035		0.080–0.082	0.18 to 0.197	0.95–1.04	6.8×10^4	(x = 5 m)

Notes: Q: initial steady flow rate; S_o = 0: horizontal bed slope; d_o, V_o: initial flow depth and mean velocity recorded at sampling location (x = 5 m in present study); U: celerity of negative surge leading edge positive upstream measured at (^{1}) x = 6 m or (^{2}) x = 5 m.

Table 2
Video movies of upstream propagation of negative surges.

Filename	Format	Description
IMGP2317.avi	HD movie (1280 × 720 pixels, 30 fps)	Experiment 130124 with PVC invert Q = 25.4 l/s, d_o = 22 cm at x = 5 m, h = 45 mm Looking downstream at the surge propagation from x = 5 m
IMGP4320.avi	HD movie (1280 × 720 pixels, 30 fps)	Experiment 130,403 with rubber mat configuration B (spikes downwards) Q = 25.4 l/s, d_o = 0.1895 m (above rubber mat) at x = 5 m, h = 64 mm Side view at x = 5 m, with initial flow direction from left to right and negative surge propagation from right to left
IMGP4322.avi	HD movie (1280 × 720 pixels, 30 fps)	Experiment 1,30,403 with rubber mat configuration B (spikes downwards) Q = 25.4 l/s, d_o = 0.1895 m (above rubber mat) at x = 5 m, h = 64 mm. Side view at x = 10.9 m, with initial flow direction from left to right and negative surge propagation from right to left
IMGP6192.avi	HD movie (1280 × 720 pixels, 30 fps)	Experiment 130719 with PVC bed Q = 34.5 l/s, d_o = 0.2035 m at x = 5 m, h = 66 mm, ADV unit at x = 10.9 m Side view at x = 10.9 m, with initial flow direction from right to left and negative surge propagation from left to right

equivalent Darcy friction factor of the rubber mat sheets was f_{matA} = 0.09–0.18 (Config. *A*) and f_{matB} = 0.05–0.09 (Config. *B*) (Fig. 4). The results were basically independent of Reynolds number, and they compared favourably with the asymptotic form of the Colebrook–White formula for fully-rough turbulent flows, called Karman–Prandtl resistance equation for turbulent flow in rough pipes [28,12]:

$$\frac{1}{\sqrt{f}} = 2.0 \times \log_{10}\left(\frac{d_H}{k_s}\right) + 1.14 \tag{4}$$

where D_H is the equivalent pipe diameter. Eq. (4) is shown in Fig. 4 and compared with the experimental data. Overall the data yielded an equivalent sand roughness height k_s = 39 mm (Config. *A*) and 12 mm (Config. *B*) on average.

2.5. Experimental flow conditions

For each experimental run, the steady gradually-varied flow conditions were established prior to sampling. The negative surge was produced by opening rapidly the tainter gate (Fig. 5). The gate

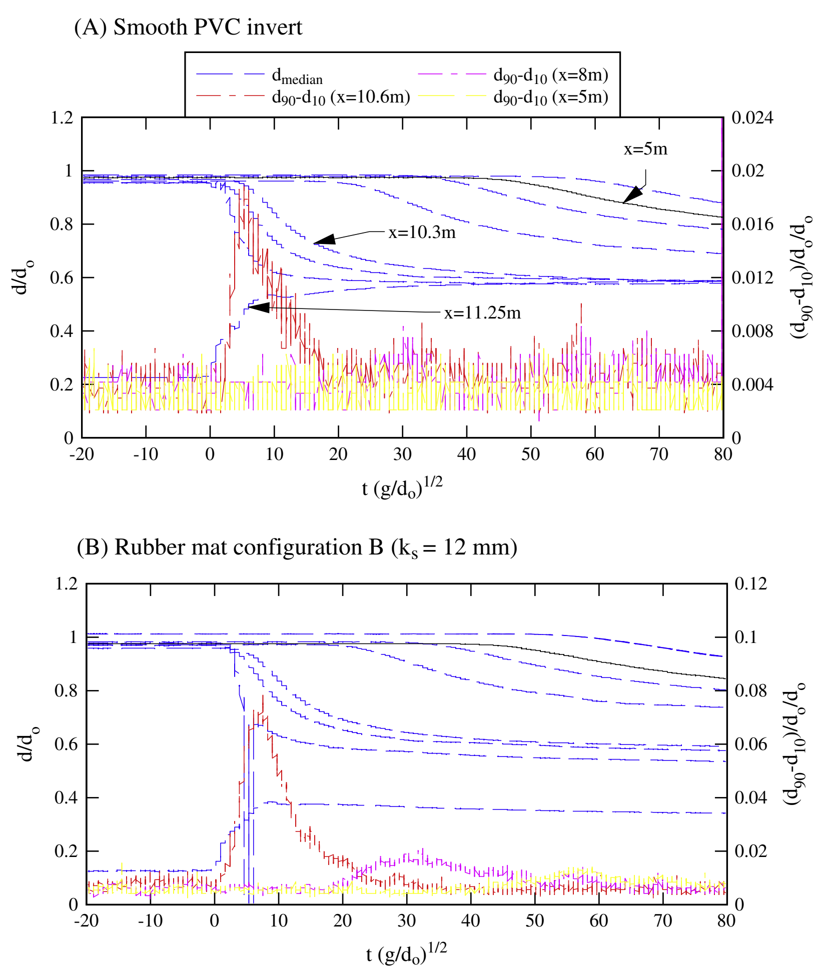

Fig. 6. Time variations of ensemble-averaged median free-surface elevations and fluctuations ($d_{90} - d_{10}$) (difference between 9th and 1st deciles) during the negative surge – flow conditions: Q = 0.0345 m^3/s, d_o = 0.182 m, h = 0.075 m – solid black line: free-surface elevation at x = 5 m.

opening time was less than 0.2 s. Such an opening time was small enough to have little effect on the negative surge propagation [16]. After opening, the gate did not intrude into the flow (Fig. 5). The experimental flow conditions are summarised in Table 1, where Q is the initially steady flow rate, d_o and V_o were recorded at $x = 5$ m, and h is the initial tainter gate opening.

The ADV unit was located at $x = 5$ m and 10.9 m (Table 1). An experimental challenge was the rapidly-varied unsteady motion (i.e. a shock). For each flow condition at each sampling location and elevation, the measurements were performed for 25 experimental runs and the results were ensemble-averaged following Bradshaw [1] and Kim and Moin [14]. A sensitivity analysis was conducted in terms of the effects of number of runs on the free-surface elevation and streamwise velocity. The time-variations of median and fluctuations were basically independent of the number of repeats for a minimum of 10–15 runs. The findings were close to the results of Perry and Watmuff [24] who needed 10 samples for convergence of the phase-averaged data. Although the number of repeats was relatively limited, it is believed that the selection of 25 runs was appropriate.

3. Basic results

3.1. Presentation

Visual, photographic and video observations were performed to investigate the upstream propagation of negative surges (Fig. 5 & Appendix A, Table 2). Fig. 5 shows two series of photographs of gate opening with nearly identical initial flow conditions on smooth and rough bed respectively. The observations highlighted the rapid gate opening (less than 0.2 s) and the negative wave formation with a relatively steep drop in water elevation in the very close vicinity of the gate. The movies IMGP4322.avi and

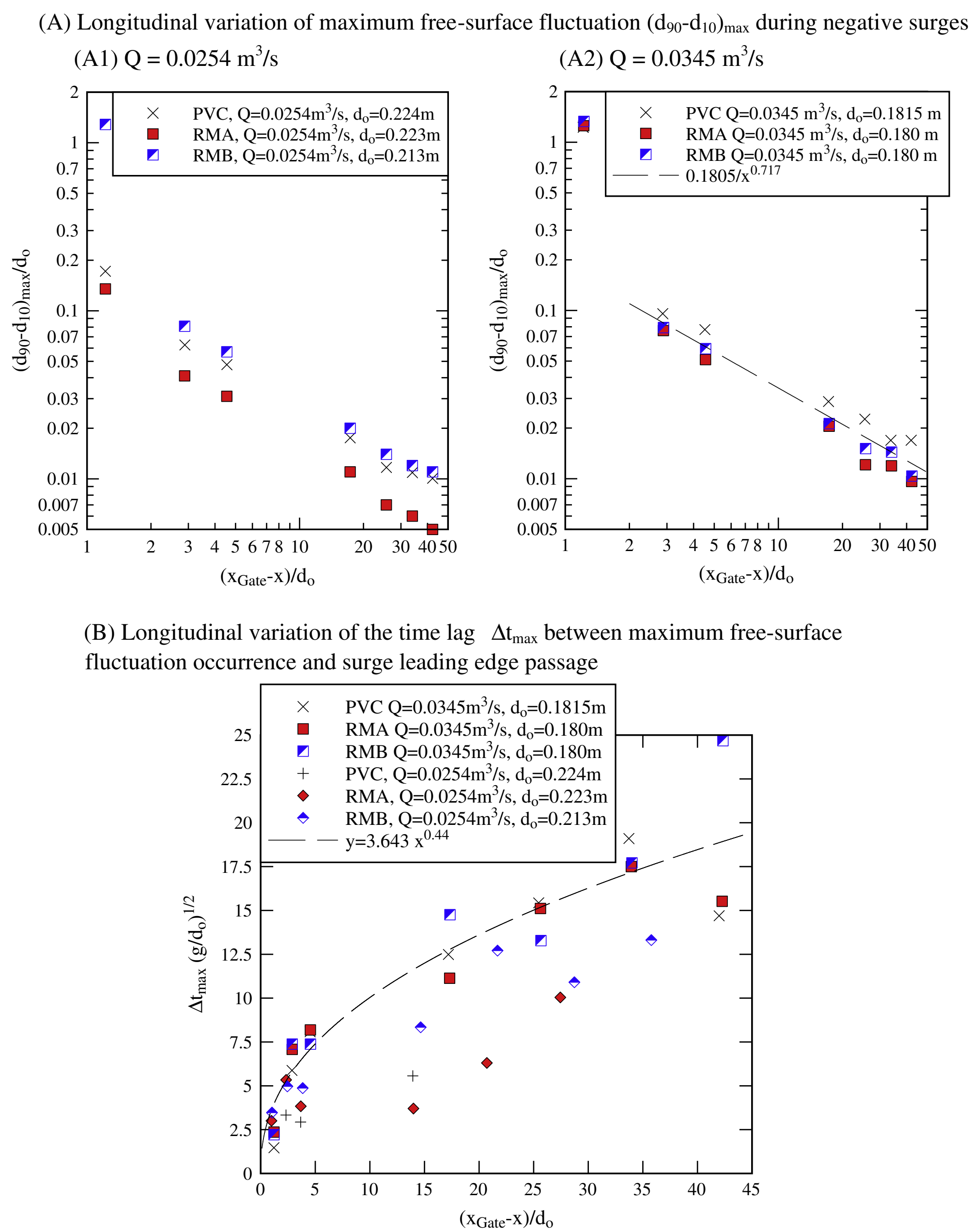

Fig. 7. Maximum free-surface fluctuations during negative surges and associated time lag.

IMGP6192.avi show the rapid opening sequence on rough and smooth bed respectively. Although some surface disturbance was seen immediately following the gate motion, these vanished very rapidly and the free-surface profile exhibited a smooth surface, within one second (movies IMGP4322.avi & IMGP6192.avi). The instantaneous free-surface profile exhibited a smooth shape as the negative surge advanced upstream (Movies IMGP2317.avi & IMGP4320.avi). In the movie IMGP2317.avi, the camera pointed downstream towards the gate and the movie highlighted the smooth water surface. The movie IMGP4320.avi illustrates the upstream surge propagation past the sampling location at $x = 5$ m. The visual observations indicated the gradual lowering of the water surface during the upstream propagation of the surge. The passage of the negative wave leading edge was barely perceptible by eye. Similar flow patterns were observed for all types of bed roughness, and further photographic observations were reported in [18].

3.2. Free-surface measurements

During the upstream propagation of the negative surge, the water depth decreased relatively gradually after the rapid generation phase. Fig. 6 illustrates some typical ensemble-averaged free-surface measurements at several longitudinal locations x, where d_o is the initial flow depth measured at $x = 5$ m. Note the different scales between the left and vertical axes in Fig. 6.

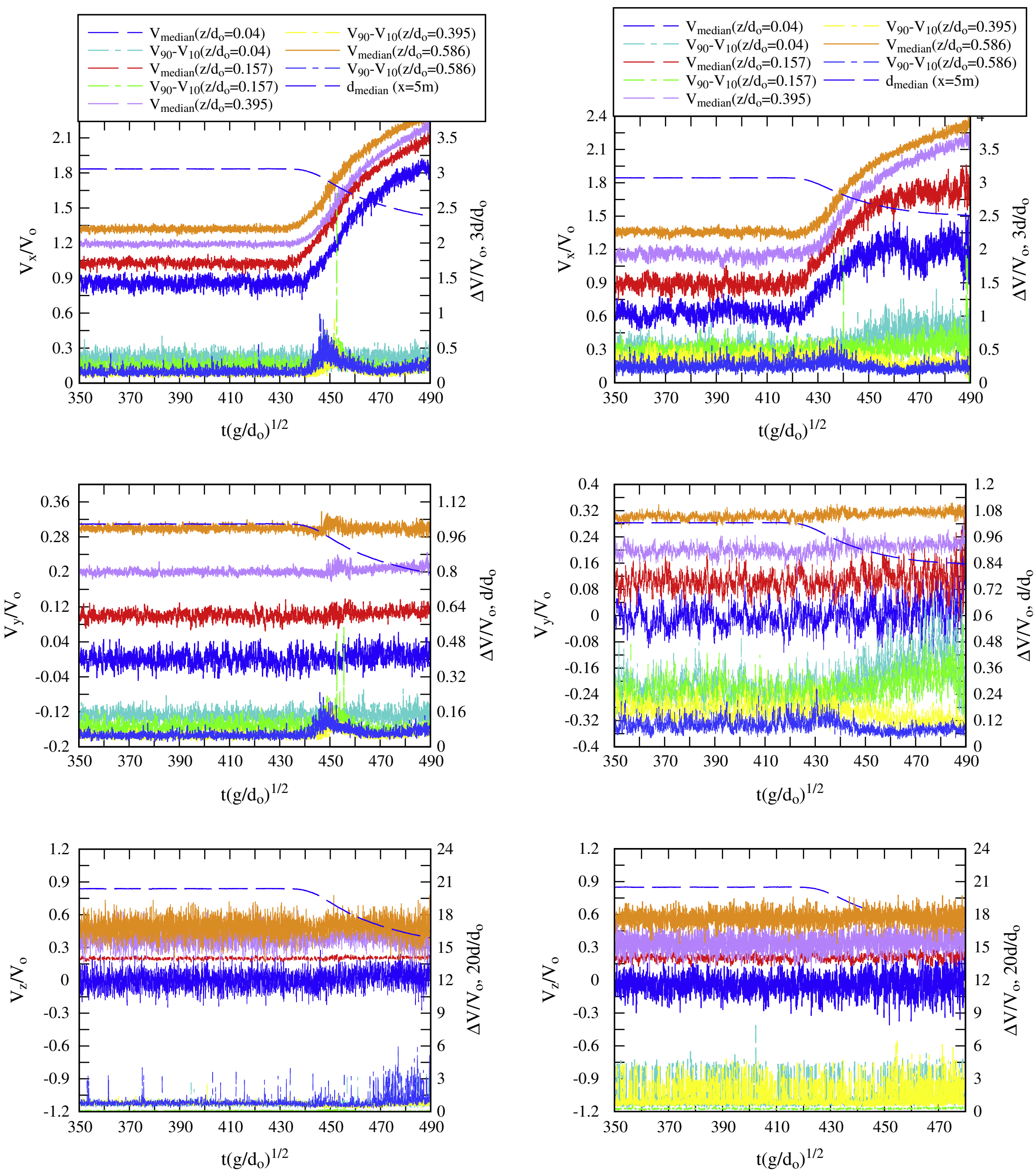

Fig. 8. Ensemble-averaged median water depth d_{median}, velocity V_{median} and velocity fluctuation ($V_{90} - V_{10}$) at $x = 5$ m recorded at different elevations during a negative surge – flow conditions: $Q = 0.0345$ m^3/s, $d_o = 0.21$ m, $x = 5$ m – left: PVC invert, right: rubber mat configuration A – median velocity data offset vertically by +0.1 for the three upper elevations.

Herein the acoustic displacement meters were sampled continuously at 200 Hz, each experiment was performed for 25 runs, the data were ensemble-averaged and $t = 0$ at the gate opening. Also the last sensor ($x = 11.25$ m) was located downstream of gate ($x_{Gate} = 11.12$ m). Its signal output recorded the positive surge generated by the rapid gate opening and propagating downstream (Fig. 6A). At all other locations, the water depth data decreased with time once the negative surge leading edge reached the sensor. The free-surface data highlighted the glossy free-surface at the surge leading edge where the free-surface curvature was more pronounced next to the gate (Fig. 6). Further upstream the free-surface slope and curvature were quantitatively small ($|\partial d/\partial x| \propto 10^{-2}$, $|\partial^2 d/\partial x^2| \propto 10^{-1}$ m^{-1}) implying that the pressure distributions were quasi-hydrostatic.

For all experiments, the data showed some relatively large free-surface fluctuations during the passage of the surge leading edge. Herein the instantaneous free-surface fluctuations were quantified in terms of the difference between the ninth and first deciles ($d_{90} - d_{10}$) of the ensemble at an instant t (Fig. 6). All the data showed a maximum in free-surface fluctuations $(d_{90} - d_{10})_{max}$ occurring slightly after the passage of the surge leading edge. The maximum free-surface fluctuations tended to decrease exponentially with increasing distance from the gate as illustrated in Fig. 6B. Typical variations with distance of $(d_{90} - d_{10})_{max}$ are reported in Fig. 7A, while Fig. 7B presents some typical time lag data Δt_{max} between the occurrence of maximum free-surface fluctuations and the passage of surge leading edge. For all three bed configurations, the maximum free-surface fluctuation $(d_{90} - d_{10})_{max}$ data showed an marked decrease with distance travelled by the surge. For $Q = 0.345$ m^3/s, the data were best fitted by

$$\frac{(d_{90} - d_{10})_{max}}{d_o} \propto \left(\frac{x_{Gate} - x}{d_o}\right)^{-0.72} \quad (x_{Gate} - x)/d_o > 2 \tag{5}$$

Some difference was observed between the two flow rates (Fig. 7A). Typically a larger free-surface fluctuation magnitude was observed next to the gate for the largest discharge, while all the data tended to similar values further upstream. The experimental data suggested further large free-surface fluctuations on the PVC bed comparable to those on the rough beds (Fig. 7). The result appeared counterintuitive but may suggest that the free-surface fluctuations were linked to the flow unsteadiness and not to the bed roughness effects. The time lag Δt_{max} showed a monotonic increase with increasing distance from the gate (Fig. 7B). Fig. 7B shows some typical dimensionless results for both discharges. Generally the dimensionless time lag was larger for the larger discharge at a given dimensionless distance from the gate. The trend was observed for all flow rates and bed configurations, and it yielded:

$$\Delta t_{max} \times \sqrt{\frac{g}{d_o}} \propto \left(\frac{x_{Gate} - x}{d_o}\right)^{0.44} \tag{6}$$

3.3. Unsteady velocity measurements

The instantaneous velocity data indicated a marked acceleration of the flow as the negative surge leading edge passed over the ADV sampling volume. The ensemble-averaged velocity data sets were analysed in terms of the ensemble-averaged median V_{median} and the instantaneous fluctuations were quantified in terms of the difference between the ninth and first deciles ($V_{90} - V_{10}$) of the data ensemble (Fig. 8). Fig. 8 presents some typical results at $x = 5$ m, where $V_o = Q/(B \times d_o)$, Q is the discharge and B is the channel width ($B = 0.5$ m). Overall the propagation of the negative surge was associated with some longitudinal acceleration and an increase in turbulent velocity fluctuations, at all vertical elevations on all three types of bed roughness. The mean flow acceleration reached $0.1 \times g$ about 0.35 m upstream of the gate, and was up to $0.01 \times g$ at $x = 5$ m, that is 6.12 m upstream of the gate. The velocity data at different elevations showed that the acceleration was comparatively larger in the upper water column (i.e. $z/d_o > 0.4$).

Close to the free-surface, some negative vertical velocity transient was observed when the water depth decreased rapidly following the passage of the surge leading edge. Relatively large negative vertical velocities were observed during the initial rapid drop in free-surface elevation (Fig. 9). Some maximum vertical velocity amplitude data are presented in Fig. 9 and compared with the maximum vertical velocity amplitude of the free-surface ($\partial d/\partial t$). Immediately upstream of the gate ($x = 10.9$ m), the maximum vertical velocity amplitudes $-(V_z)_{max}/V_o$ were large, reaching values close to unity (Fig. 9), although $-(V_z)_{max}/V_o$ was much smaller further upstream. The maximum vertical velocity amplitudes decreased with decreasing vertical elevations, tending to zero at the invert ($z = 0$), as implied by the no-flow-through boundary condition for an impervious boundary.

Some distinct peaks in velocity fluctuations were highlighted at higher vertical elevations ($z/d_o \geqslant 0.04$) on all three bed configurations following the passage of the surge leading edge (Fig. 8). At a given vertical elevation, the maximum velocity fluctuations were smaller on the rougher beds compared to those recorded on the smooth bed. Next to the gate ($x = 10.9$ m), the velocity data showed a same trend than that observed at $x = 5$ m. But the magnitude of the longitudinal acceleration, the turbulent velocity fluctuations and the vertical velocity magnitude were larger in terms of the absolute values, in comparison to the results at $x = 5$ m.

4. Discussion

In a rapidly-varied unsteady flow, the instantaneous velocity fluctuation V_i is the deviation between the measured velocity and the ensemble-average [1]:

$$V_i = V_i - \overline{V_i} \tag{7}$$

where V_i is the instantaneous velocity component data, $\overline{V_i}$ is the instantaneous ensemble-average median value herein and $i, j = x$,

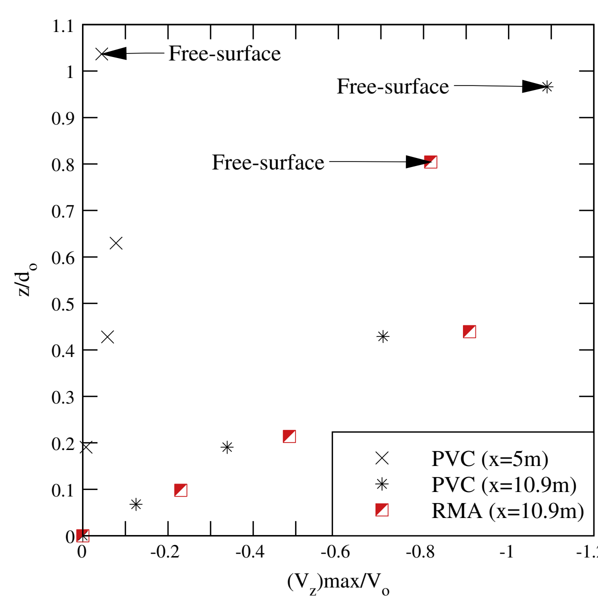

Fig. 9. Maximum negative ensemble-averaged median vertical velocity during the passage of the negative surge leading edge – flow conditions: $Q = 0.0345$ m^3/s, $d_o = 0.21$ m, $x = 5$ m & 10.9 m – comparison with the maximum free-surface vertical velocity $\partial d/\partial t$.

y, z. Thus the turbulent stress tensor component equals: $\tau_{ij} = \rho \times v_i \times v_j$. In the present study, the velocity measurements were performed 25 times at both locations. For each experimental flow condition and vertical elevation z, the ensemble-averaged data were calculated. Typical results were shown in Fig. 10, where the time variations of ensemble-averaged median normal and tangential stresses are presented in dimensionless form and compared with the ensemble-averaged median water depth.

The results showed overall large Reynolds stress magnitudes and rapid fluctuations beneath the negative surge. The magnitude of the turbulent stresses was larger than in the initially steady flow. This is illustrated in Fig. 10. While the boundary shear stress in an accelerating flow is lower than that in a steady flow for the same velocity and depth [9], the present data showed larger shear stress levels in the accelerating flow. The present findings were observed for all turbulent stress tensor components, for all types of bed roughness and at all elevations within the water column, although larger stress levels tended to be observed next to the bed. In the mid to upper water column, most Reynolds stresses exhibited a distinct peak in turbulent shear stress magnitude $(\tau_{ij})_{max}$ shortly after the passage of the negative surge leading edge (Fig. 10). The finding implied some very intense mixing within the water column. The peak of Reynolds stresses was not clearly evident next the bed (i.e. $z/d_o < 0.15$). Close to the bed, the data

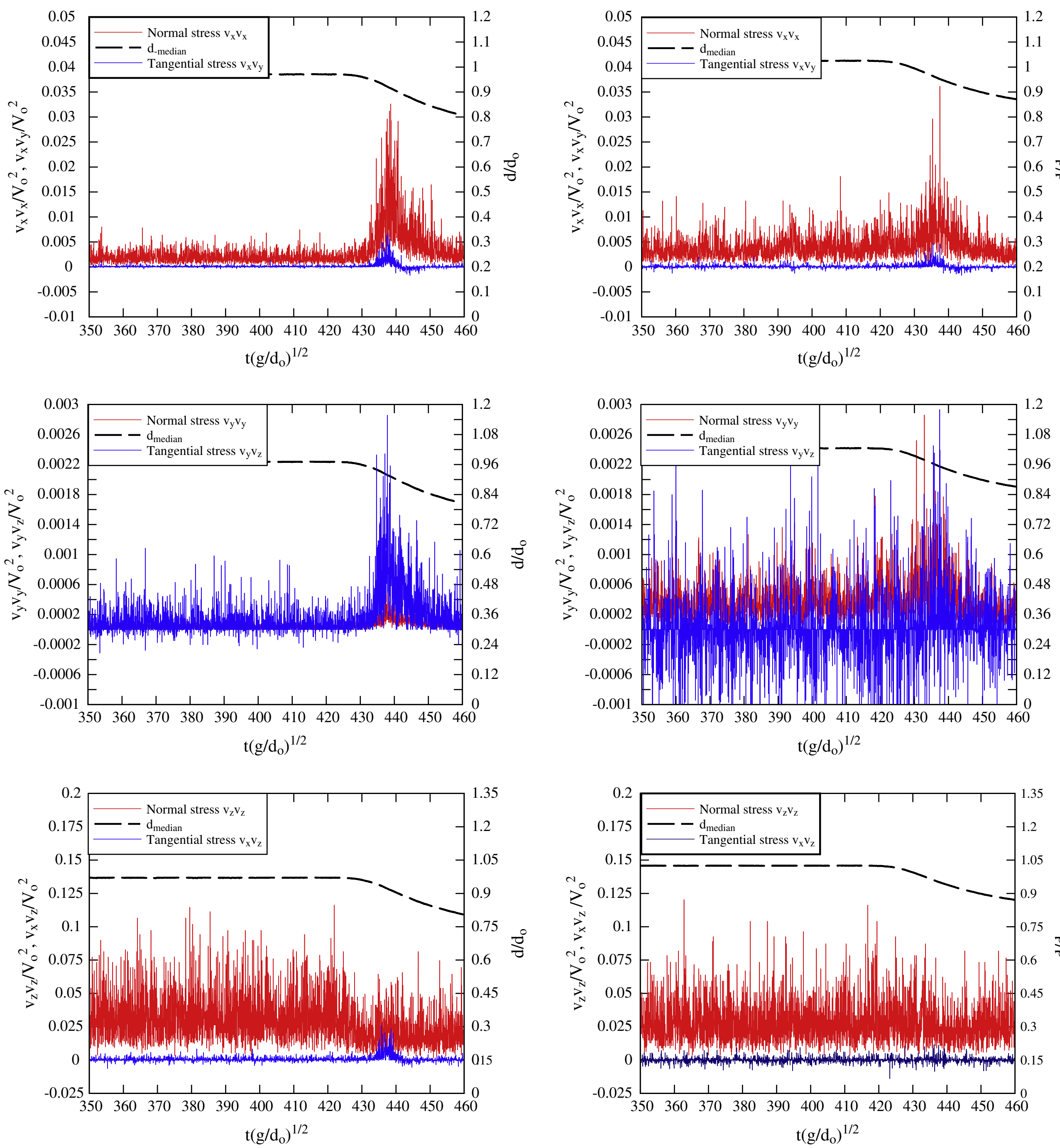

Fig. 10. Ensemble-averaged median water depth d_{median} and median turbulent stress components in the upper water column during a negative surge propagation – flow conditions: $Q = 0.0345\ m^3/s$, $d_o = 0.21$ m, $x = 5$ m. (A, left) smooth PVC invert, $d_o = 0.205$ m, $z/d_o = 0.628$. (B, right) rubber mat configuration A, $d_o = 0.212$, $z/d_o = 0.652$.

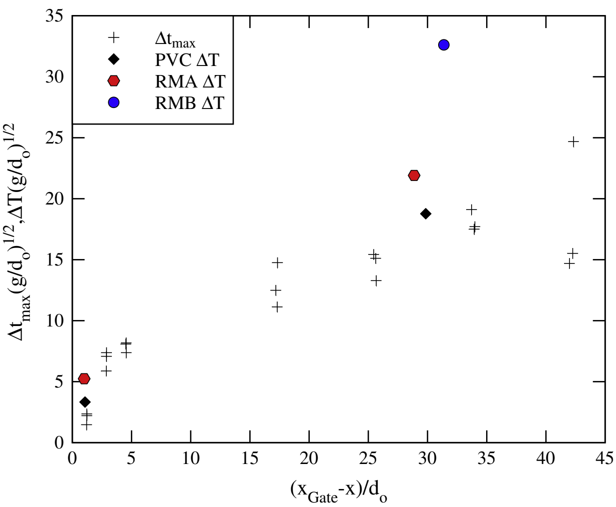

Fig. 11. Longitudinal variation of the average time lag ΔT between maximum shear stress occurrence and surge leading edge passage – comparison with the time lag Δt_{max} between maximum free-surface fluctuation occurrence and surge leading edge passage.

indicated an increase in Reynolds stress amplitudes following the negative surge propagation and free-surface elevation lowering.

The maximum shear stress component $(\tau_{ij})_{max}$ and the time delay ΔT_{ij} between the passage of negative surge leading edge and the occurrence of shear stress maximum were estimated for all data sets (Appendix B). The results in terms of time delay ΔT between the passage of negative surge leading edge and the occurrence of shear stress maximum were close for all shear stress components, with little difference between the three types of bed roughness. The averaged data are presented in Fig. 11 as functions of the distance $(x_{Gate} - x)$ from the gate, where x_{Gate} = 11.12 m. The data are compared with the time lag Δt_{max} between maximum free-surface fluctuation occurrence and surge leading edge passage in Fig. 11. The comparison indicated a close agreement, suggesting that the maximum free-surface fluctuations were linked to the occurrence of maximum shear stress in the water column, especially close to the free-surface.

5. Conclusion

The unsteady turbulent flow induced by a negative surge was investigated experimentally in a relatively large rectangular channel. Both unsteady free-surface profiles and velocity characteristics were measured in a negative surge propagating upstream following a rapid gate opening. Three types of bed roughness were tested systematically: smooth PVC and two rough beds. All measurements of free-surface and velocity components were performed 25 times and the results were ensemble-averaged.

The propagation of the negative surge was smooth and barely perceptible, but very close to the gate. Relatively large free-surface fluctuations and turbulent velocity fluctuations were recorded beneath the leading edge of the negative surge. The free-surface fluctuations decreased exponentially with increasing distance from the gate for all flow conditions and bed configurations. The time delay between the occurrence of maximum free-surface fluctuations and passage of surge leading edge was observed to increase monotonically with increasing distance from the gate, and it was comparable to the time delay for the occurrence of maximum Reynolds stresses. The finding suggested that the maximum free-surface fluctuations were closely linked to the occurrence of maximum shear stress in the water column especially close to the free-surface. The experimental data showed a rapid flow acceleration beneath the negative surge. Large and rapid fluctuations in all instantaneous velocity components were observed during the passage of the negative surge leading edge. The instantaneous Reynolds stress data showed also large fluctuations, significantly larger than in the initially steady flow. Altogether the results highlighted the complexity of the unsteady mixing beneath negative surges in a simple channel geometry (i.e. prismatic rectangular).

A key finding was the limited amount of qualitative and quantitative difference between all types of roughness, encompassing both smooth boundary (PVC) and very rough boundary (RMA & RMB) conditions. Herein the unsteady time scale was less than a second. In contrast, the response time of the bed roughness to the shock was longer. In the classical experiments of Logan and Jones [21], the response of the flow turbulence to an abrupt change in boundary conditions took place over a distance of 4–8 pipe diameters, in terms of the inner flow properties and more than 15 pipe diameters for the centerline properties [17]. Using DNS calculations in a rapidly accelerating channel. He et al. [10] demonstrated that the turbulent response to the stepwise acceleration was a delayed process: "*this process takes a considerable period of time*". They reported a dimensionless turbulence response time $t \times d/V$ between 5 and 40: at the present experimental scale, this would corresponds between 2 and 8 s. Simply the hydraulic transient was a shock, i.e. highly unsteady non-periodic flow motion, with a characteristic time scale much shorter than the response time of the invert boundary roughness on the accelerating flow conditions. Thus the bed roughness had little impact on the unsteady surge flow characteristics.

Acknowledgments

The authors thank Professor Fabian Bombardelli (University of California Davis, USA) and Dr. Mario Franca (Ecole Polytechnique Fédérale de Lausanne, Switzerland) for their advice. They acknowledge all the people who assisted with the large-scale experiments and the technical staff of the School of Civil Engineering at the University of Queensland, in particular Mrs. Simin Sun, Mr. Jason Van Der Gevel and Mr. Stewart Matthews. The financial support of the Australian Research Council (Grant DP120100481) is acknowledged. Lastly the authors thank the two reviewers for their helpful comments and advice.

Appendix A. Video movies of air bubble motion inside the gabions

The negative surge was a rapidly-varied unsteady flow motion. The upstream propagation of the surge was documented with a series of video movies taken with a digital SLR camera Pentax^{TM} K-7 during some experiments. The list of movies is detailed in Table 2.

Appendix B. Maximum instantaneous shear stress beneath negative surges and their occurrence

The instantaneous ensemble-averaged Reynolds stresses presented typically a maximum shortly after the passage of the negative surge leading edge (Fig. 10). The maximum shear stress component $(\sigma_{ij})_{max}$ and the time delay ΔT_{ij} between the passage of negative surge leading edge and the occurrence of shear stress maximum were recorded for all data sets, where $\sigma_{ij} = \rho \times v_i \times v_j$ and $i, j = x, y, z$. Table 3 regroups the results calculated in terms of the instantaneous data. Note that the time delay ΔT_{ij} was

Table 3
Maximum instantaneous shear stresses beneath negative surges and their occurrence (Present study).

Q (m^3/s) (1)	Bed (2)	d_o (m) (3)	x_{ADV} (m) (4)	d_{ADV} (m) (5)	z (m) (6)	Maximum stress [a]						Time delay [b]					
						$(\sigma_{xx})_{max}$ (Pa) (7)	$(\sigma_{yy})_{max}$ (Pa) (8)	$(\sigma_{zz})_{max}$ (Pa) (9)	$(\sigma_{xy})_{max}$ (Pa) (10)	$(\sigma_{xz})_{max}$ (Pa) (11)	$(\sigma_{yz})_{max}$ (Pa) (12)	ΔT_{xx} (s) (13)	ΔT_{yy} (s) (14)	ΔT_{zz} (s) (15)	ΔT_{xy} (s) (16)	ΔT_{xz} (s) (17)	ΔT_{yz} (s) (18)
0.0345	PVC	0.205	5.00	0.2	0.0138	4.64	0.902	N/A	0.549	3.00	1.68	4.84	3.23	N/A	3.38	3.34	4.18
0.0345	PVC	0.205	5.00	0.2	0.0388	5.785	0.488	N/A	0.527	2.86	1.50	2.53	1.98	N/A	2.65	2.95	2.76
0.0345	PVC	0.205	5.00	0.2	0.0888	3.17	0.34	9.804	0.565	2.16	1.50	2.65	2.44	2.55	2.30	2.30	2.44
0.0345	PVC	0.205	5.00	0.2	0.1288	3.515	0.349	9.198	0.726	4.02	1.60	2.19	2.02	2.00	2.08	2.21	2.12
0.0345	RMA	0.212	5.00	0.2	0.02334	N/A	N/A	N/A	N/A	N/A	N/A	N/A	N/A	N/A	N/A	N/A	N/A
0.0345	RMA	0.212	5.00	0.2	0.04834	N/A	N/A	N/A	N/A	N/A	N/A	N/A	N/A	N/A	N/A	N/A	N/A
0.0345	RMA	0.212	5.00	0.2	0.09834	4.42	0.97	N/A	0.741	N/A	1.58	2.57	1.79	N/A	2.42	N/A	4.13
0.0345	RMA	0.212	5.00	0.2	0.13834	3.90	0.488	14.371	0.534	1.24	1.00	2.85	2.19	9.39	2.55	2.67	2.85
0.0345	RMB	0.195	5.00	0.2	0.01534	N/A	N/A	N/A	N/A	N/A	N/A	N/A	N/A	N/A	N/A	N/A	N/A
0.0345	RMB	0.195	5.00	0.2	0.04034	13.67	1.36	N/A	1.40	N/A	5.70	5.57	6.04	N/A	6.59	N/A	5.17
0.0345	RMB	0.195	5.00	0.2	0.09034	7.21	0.784	N/A	0.67	7.31	3.03	4.25	4.70	N/A	3.66	3.84	4.70
0.0345	RMB	0.195	5.00	0.2	0.13034	10.06	0.813	*714.28*	2.96	10.72	3.61	3.36	3.36	7.22	3.36	3.36	3.93
0.0345	PVC	0.206	10.90	0.2	0.0138	7.67	N/A	N/A	0.317	N/A	N/A	0.61	N/A	N/A	0.34	N/A	N/A
0.0345	PVC	0.206	10.90	0.2	0.0388	4.32	6.84	19.28	−2.13	−1.735	1.34	0.20	0.43	0.35	0.44	0.40	0.35
0.0345	PVC	0.206	10.90	0.2	0.0888	3.11	0.339	28.49	−0.43	2.44	2.54	0.85	0.35	0.95	0.14	0.88	0.30
0.0345	RMA	0.221	10.90	0.2	0.0222	5.701	N/A	N/A	N/A	N/A	N/A	0.08	N/A	N/A	N/A	N/A	N/A
0.0345	RMA	0.221	10.90	0.225	0.0472	6.625	1.644	14.12	N/A	N/A	1.42	0.46	0.48	0.46	N/A	N/A	0.47
0.0345	RMA	0.221	10.90	0.225	0.0972	2.82	0.98	25.24	−0.55	2.38	1.24	1.07	1.10	1.14	0.57	0.95	1.14

Notes: N/A: no distinctive peak.
[a] Instantaneous ensemble-averaged median.
[b] Data estimated based upon the smoothed instantaneous ensemble-averaged Reynolds stress data sets; *Italic*: suspicious data.

estimated based upon the smoothed data sets to minimise any potential bias.

Appendix C. Supplementary material

Supplementary data associated with this article can be found, in the online version, at http://dx.doi.org/10.1016/j.expthermflusci.2014.06.015.

References

[1] P. Bradshaw, An Introduction to Turbulence and its Measurement, The Commonwealth and International Library of Science and technology Engineering and Liberal Studies, Thermodynamics and Fluid Mechanics Division, Pergamon Press, Oxford, UK, 1971. 218 pages.

[2] British Standard, Flow Measurement, British Standard Institution, London, 1943. British Standard Code BS 1042:1943.

[3] H. Chanson, Environmental Hydraulics of Open Channel Flows, Elsevier-Butterworth-Heinemann, Oxford, UK, 2004, p. 483.

[4] H. Chanson, Applied Hydrodynamics: An Introduction, CRC Press, Taylor & Francis Group, Leiden, The Netherlands, 2014, p. 448. 21 video movies.

[5] H. Chanson, N.J. Docherty, Turbulent velocity measurements in open channel bores, Euro. J. Mech. B/Fluids 32 (2012) 52–58, http://dx.doi.org/10.1016/j.euromechflu.2011.10.001. ISSN 0997-7546.

[6] L. Djenidi, R. Elavarasan, R.A. Antonia, The turbulent boundary layer over transverse square cavities, J. Fluid Mech. 395 (1999) 271–294.

[7] H. Favre, Etude Théorique et Expérimentale des Ondes de Translation dans les Canaux Découverts (Theoretical and Experimental Study of Travelling Surges in Open Channels), Dunod, Paris, France, 1935 (in French).

[8] D.G. GORING, V.I. NIKORA, Despiking acoustic doppler velocimeter data, J. Hydraul. Eng., ASCE 128 (1) (2002) 117–126. Discussion: Vol. 129, No. 6, pp. 484-489.

[9] S. He, C. Ariyaratne, A.E. Vardy, Wall shear stress in accelerating turbulent pipe flow, J. Fluid Mech. 685 (2011) 440–460, http://dx.doi.org/10.1017/jfm.2011.328.

[10] S. He, M. Seddighi, Turbulence in transient channel flow, J. Fluid Mech. 715 (2013) 60–102.

[11] F.M. Henderson, Open Channel Flow, MacMillan Company, New York, USA, 1966.

[12] I.E. IDELCHIK, Handbook of Hydraulic Resistance, third ed., CRC Press, Boca Raton, USA, 1994, p. 790.

[13] N. Khezri, H. Chanson, Undular and breaking tidal bores on fixed and movable gravel beds, J. Hydraul. Res., IAHR 50 (4) (2012) 353–363, http://dx.doi.org/10.1080/00221686.2012.686200.

[14] J. Kim, P. Moin, The structure of the vorticity field in turbulent channel flow. Part 2. study of ensemble-averaged fields, J. Fluid Mech. 162 (1986) 339–363.

[15] C. Koch, H. Chanson, Turbulence measurements in positive surges and bores, J. Hydraul. Res., IAHR 47 (1) (2009) 29–40, http://dx.doi.org/10.3826/jhr.2009.2954.

[16] G. Lauber, Experimente zur talsperrenbruchwelle im glatten geneigten rechteckkanal. Dam Break Wave Experiments in Rectangular Channels, Ph.D. thesis, VAW-ETH, Zürich, Switzerland, 1997, (also Mitteilungen der Versuchsanstalt fur Wasserbau, Hydrologie und Glaziologie, ETH-Zurich, Switzerland, No. 152) (in German).

[17] J. Laufer, Flow in a pipe following an abrupt increase in surface roughness – discussion, J. Basic Eng., ASME 85 (1) (1963) 9.

[18] X. Leng, H. Chanson, Propagation of Negative Surges in Rivers and Estuaries: Unsteady Turbulent Mixing and the Effects of Bed Roughness, Hydraulic Model Report No. CH93/13, School of Civil Engineering, The University of Queensland, Brisbane, Australia, 2014, p. 108 (ISBN 9781742720999).

[19] J. LEWIN, Hydraulic Gates and Valves in Free Surface Flow and Submerged Outlets, Thomas Telford, London, 1985, p. 238.

[20] J.A. Liggett, Fluid Mechanics, McGraw-Hill, New York, USA, 1994.

[21] E. Logan, J.B. Jones, Flow in a pipe following an abrupt increase in surface roughness, J. Basic Eng., ASME 85 (1) (1963) 35–38.

[22] J.S. Montes, Irrotational flow and real fluid effects under planar sluice gates, J. Hydraul. Eng., ASCE 123 (3) (1997) 219–232.

[23] J.S. MONTES, Hydraulics of Open Channel Flow, ASCE Press, New-York, USA, 1998, p. 697.

[24] A.E. Perry, J.H. Watmuff, The phase-averaged large-scale structures in three-dimensional turbulent wakes, J. Fluid Mech. 103 (1981) 33–61.

[25] A.J. Raudkivi, R.A. Callander, Analysis of Groundwater Flow, Edward Arnold Publisher, London, UK, 1976.

[26] M. Reichstetter, H. Chanson, Unsteady turbulent properties in negative waves in open channels, Euro. J. Mech. B/Fluid 37 (2013) 1–9, http://dx.doi.org/10.1016/j.euromechflu.2012.07.003. 2 video movies.

[27] M. Reichstetter, H. Chanson, Negative surges in open channels: physical and numerical modeling, J. Hydraul. Eng., ASCE 139 (3) (2013) 341–346, http://dx.doi.org/10.1061/(ASCE)HY.1943-7900.0000674.

[28] H. ROUSE, Elementary Mechanics of Fluids, John Wiley & Sons, New York, USA, 1946, p. 376.

[29] T.W. Sturm, Open Channel Hydraulics, Water Resources and Environmental Engineering Series, McGraw Hill, Boston, USA, 2001, p. 493.

[30] L. TAN, V.H. CHU, Lauber and hager's dam-break wave data for numerical model validation, J. Hydrol. Res., IAHR 47 (4) (2010) 524–528.

[31] T.L. WAHL, Despiking acoustic doppler velocimeter data. discussion, J. Hydrol. Eng., ASCE 129 (6) (2003) 484–487.